Journal of Power Sources 248 (2014) 560–564

Contents lists available at ScienceDirect

Journal of Power Sources

journal homepage: www.elsevier.com/locate/jpowsour

Short communication

Hydrogen evolution at the negative electrode of the all-vanadium redox flow batteries

Che-Nan Sun [a,*], Frank M. Delnick [b], Loïc Baggetto [a], Gabriel M. Veith [a], Thomas A. Zawodzinski Jr. [a,c,d,*]

[a] Materials Science and Technology Division, Oak Ridge National Laboratory, Oak Ridge, TN 37831, USA
[b] Power Sources Technology Group, Sandia National Laboratory, Albuquerque, NM 87185, USA
[c] Department of Chemical and Biomolecular Engineering, University of Tennessee, Knoxville, TN 37996, USA
[d] Department of Chemistry, King Abdulaziz University, Jeddah, Saudi Arabia

HIGHLIGHTS

- The rate of hydrogen evolution in the all-vanadium redox flow battery (VRFB) is quantified.
- The method for determining the electrochemical surface area of the VRFB electrode is proposed.
- Higher surface area electrode leads to a higher hydrogen evolution rate.

ARTICLE INFO

Article history:
Received 23 August 2013
Received in revised form
27 September 2013
Accepted 29 September 2013
Available online 6 October 2013

Keywords:
Hydrogen evolution
Redox flow battery
Side reaction
Electrochemical surface area

ABSTRACT

This work demonstrates a quantitative method to determine the hydrogen evolution rate occurring at the negative carbon electrode of the all vanadium redox flow battery (VRFB). Two carbon papers examined by buoyancy measurements yield distinct hydrogen formation rates (0.170 and 0.005 μmol min^{-1} g^{-1}). The carbon papers have been characterized using electron microscopy, nitrogen gas adsorption, capacitance measurement by electrochemical impedance spectroscopy (EIS), and X-ray photoelectron spectroscopy (XPS). We find that the specific electrochemical surface area (ECSA) of the carbon material has a strong influence on the hydrogen generation rate. This is discussed in light of the use of high surface area material to obtain high reaction rates in the VRFB.

Published by Elsevier B.V.

1. Introduction

There is increasing recognition of the need for large-scale energy storage systems for effectively integrating intermittent and renewable energy sources to the modern electrical grid. [1,2] The redox flow battery (RFB), which provides a highly scalable method of energy storage, is one promising technology for this application and has therefore attracted a great deal of attention in recent years. [3–5] The all-vanadium redox flow battery (VRFB) [6–10] is a type of RFBs that employs four different oxidation states of vanadium ions, V^{2+}/V^{3+} and V^{4+}/V^{5+} in two reaction compartments which are separated by an ion-conducting membrane, to serve as the redox couples for the negative and the positive electrode reactions, respectively.

Despite the apparent simplicity of the involved electrochemical reactions, optimizing the RFB is in reality very complex. Efforts have been made toward improving the VRFB performance by modifying electrodes, [11–15] membranes, [16–19] electrolytes, [7,20] and cell configuration. [13] However, self-discharge induced by vanadium ion crossover [21] and the tendency to develop asymmetrical valence of vanadium ion in positive and negative electrolytes due to side reactions [22–24] are two important system challenges. Recently, vanadium crossover through the membrane was effectively reduced by altering the polymer morphology [25] or employing anion exchange membranes. [19,26] However, the impact of the side reactions on VRFB operation still remains to be addressed.

We recently demonstrated the possibility of integrating a reference electrode into the VRFB. [27,28] The presence of a reference electrode enabled us to separate and individually study the electrochemical processes on the positive and negative electrodes.

* Corresponding authors. Materials Science and Technology Division, Oak Ridge National Laboratory, Oak Ridge, TN 37831, USA
E-mail addresses: sunc@ornl.gov, chenan.sun@gmail.com (C.-N. Sun), tzawodzi@utk.edu (T.A. Zawodzinski).

0378-7753/$ – see front matter Published by Elsevier B.V.
http://dx.doi.org/10.1016/j.jpowsour.2013.09.125

From that work, we see that the potential of the negative electrode lays ca. 350 mV below that of a dynamic hydrogen reference electrode at 50% state of charge (SoC). [27,28] The lower potential thermodynamically allows for simultaneous hydrogen evolution reaction (HER) and V^{2+}/V^{3+} reactions on the negative side of the cell. Moreover, we also observed a significant amount of gas generated by plunging a piece of platinum foil into the negative electrolyte. The magnitude of the thermodynamic driving force of the HER depends on the proton concentration and the SoC according to the Nernst equation. Since vanadium ions are typically dissolved in concentrated (3–5 M) sulfuric acid, the Nernst potential for the hydrogen evolution shifts positively due to the high proton concentration. On the other hand, the Nernst potential of the V^{2+}/V^{3+} couple becomes more negative as the SoC increases, thereby increasing the driving force for the HER.

In this work, we demonstrate a simple protocol to evaluate quantitatively the impact of the carbon paper electrode material on the gas evolution side reaction. The protocol is based on a combination of buoyancy measurement and characterization techniques (electron microcopy, gas adsorption, ECSA, XPS) to probe the crucial material properties (surface area and chemistry) affecting the rate of the side reactions.

2. Experiment

2.1. Material

Two commercially available carbon papers were used in this study: carbon paper (10AA, SGL) and carbon paper with enhanced surface area (CP-ESA, SGL).

2.2. Scanning electron microscopy (SEM)

The structure and morphology of the carbon samples were characterized using a Hitachi S-4800 scanning electron microscope.

2.3. Buoyancy

The negative electrolyte at high state of charge (SoC), i.e. mostly vanadium (II), was adopted for this experiment. Electrolyte with the concentration of 1.7 M vanadium in 3.3 M sulfuric acid was prepared by adopting the electrochemical procedure described elsewhere. [28] Carbon samples with 2 mL of electrolyte were sealed under nitrogen in a pouch. The pouch with a weight attached at the bottom was subsequently hung from a balance with a nickel wire and fully immersed into DI water with the top of the pouch c.a. 1 inch below the water surface (Fig. S1a). The reading of the balance was recorded periodically within an 8-h window. The system was kept in a closed box to avoid weighing error caused by the air circulation. The temperature of the water bath was 20 °C.

2.4. Mass spectroscopy

Analysis of the gas products formed in the cells was performed using an Ametek Dymaxion Mass Spectrometer (0–200 amu) using He as carrier gas. Briefly, samples were collected using a gas tight syringe (Aldrich), which was flushed with argon gas prior to sampling, and immediately injected into the mass spectrometer through a Supelco Septum into the He gas.

2.5. Surface area

The surface area was determined using a Quantachrome Autosorb 1 BET system. Prior to measurement, the samples were degassed at elevated temperature under vacuum until the pressure rise was sufficiently low. Subsequently, the samples were rapidly transferred to the gas adsorption station for the experiments. The adsorbed volume of nitrogen in the samples was measured at relative pressures (applied pressure normalized by ambient pressure) over the range from 4×10^{-5} to slightly less than 1.0 at 77 K.

2.6. X-ray photoelectron spectroscopy (XPS)

Surface chemistry was probed using a PHI 3056 spectrometer equipped with an Al K_α source (1486.6 eV) in a cryo-pumped vacuum chamber with a measurement pressure below 10^{-8} Torr. High resolution scans were taken at 350 W with 23.5 eV pass energy and 0.05 eV energy step, and survey scans were measured at 350 W with 93.9 eV pass energy and 0.3 eV energy step. The binding energies were shifted to account for charging by setting the most intense carbon signal to 284.8 eV. The intensities of the presented spectra were not normalized and are simply shifted vertically for clarity. Surface concentrations are calculated by integrating the peak areas and using standard atomic sensitivity factors supplied by the equipment manufacturer. Assignments are based on fitting the data using Gaussian–Lorentzian functions and a Shirley-type background.

2.7. Capacitance

Two Nafion 117 membrane sandwiched by two carbon papers were assemble into a “zero-gap” cell. [13] The $Hg/HgSO_4$ electrode was adopted as the reference electrode, with its tip contacting the Nafion overhanging the cell hardware. The contact point was wetted with 0.5 M H_2SO_4 to improve ion conduction. The electrode compartments were then filled with 4 M sulfuric acid using a peristaltic pump. EIS was measured at the open circuit potential (OCP) with respect to the reference electrode. The capacitance of the carbon paper electrode was obtained by fitting the capacitance tail obtained with EIS to an equivalent circuit model consisting of a constant phase element (CPE) in series with a resistor (Fig. S2).

3. Results and discussion

3.1. Carbon paper morphology

SEM images showing the structure and morphology of the carbon samples are presented in Fig. 1. The carbon papers adopted in this study are comprised of a fiber matrix with various fillers. The filler morphology is shown in the inset images. The characteristics of the carbon paper are primarily dominated by the properties and the structure of the filler. For instance, it is obvious that the carbon filler in CP-ESA has a finer structure as compared to those in 10AA. The finer structure induces higher BET surface area (BETSA) as summarized in Table 1.

3.2. Hydrogen evolution rate

Buoyancy experiments were carried out to measure the rate of gas generation. A control experiment (without the carbon sample) was initially conducted confirming that the contribution of the pouch material is negligible (Fig. S1b). Depending on the material, an appropriate sample quantity, determined during preliminary tests, was employed to ensure a sufficient volume change with negligible electrolyte concentration variation during the testing period. With the presence of the carbon paper, the pouch gradually expands due to the gas formation and the apparent immersed weight during the buoyancy measurement decreases according to Archimedes' principle. Assuming the apparent immersed weight change is primarily attributed to water displacement, the volume of the generated gas can be estimated with known water density.

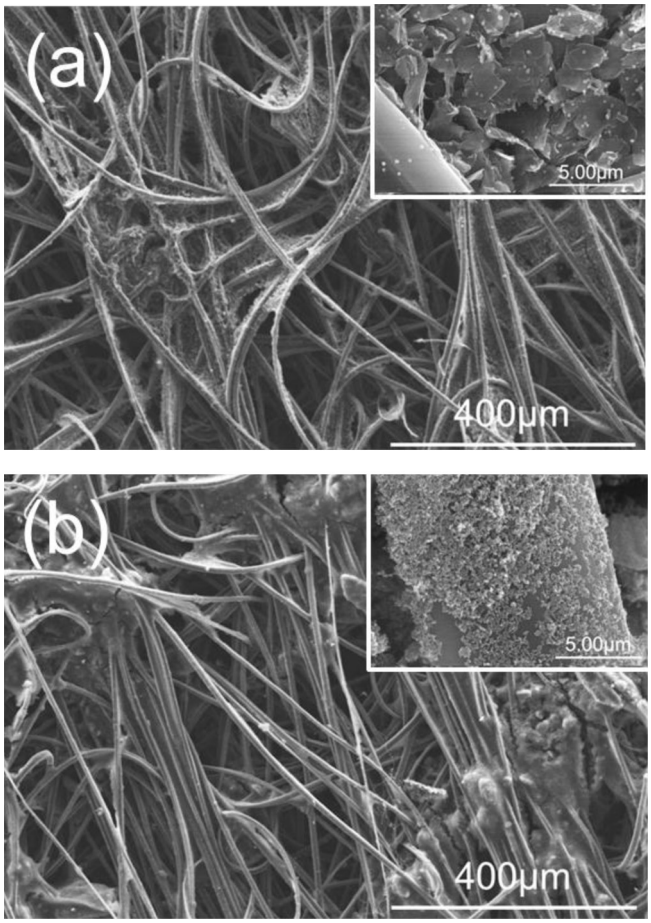

Fig. 1. SEM micrographs of the carbon fiber samples (a) 10AA (b) CP-ESA Inset: micrograph of the filler.

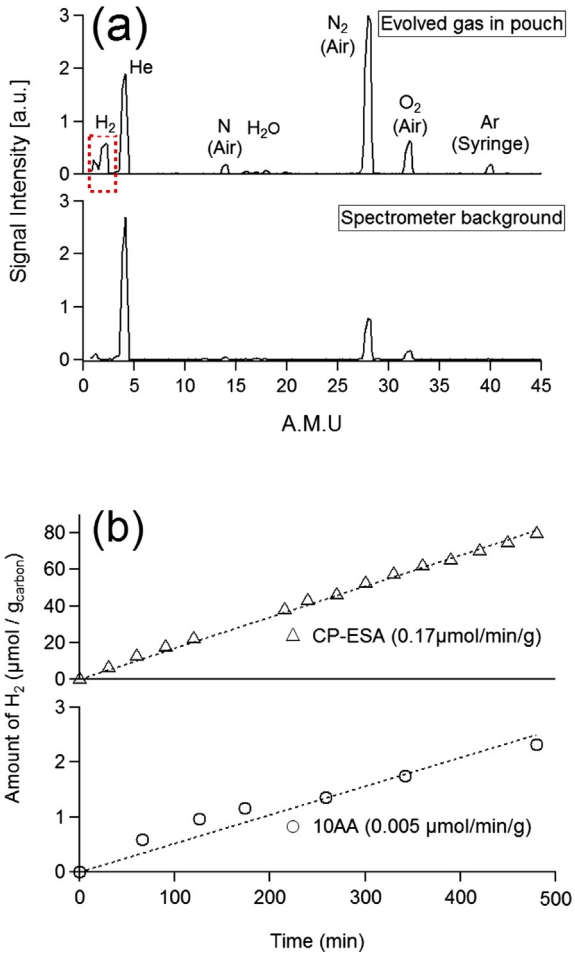

Fig. 2. (a) Mass spectra of the analyzed gases. Top graph: gas sampled from the headspace of the expanded pouch. Bottom graph: reference spectrum showing the gas in the spectrometer. (b) Amounts of hydrogen in moles that are generated as a function of time for CP-ESA and 10AA. Dash line: fitting.

Subsequently, the amount of gas can be estimated using the ideal gas law with the measured water bath temperature. The gas sampled from the headspace of the expanded pouch was analyzed using a mass spectrometer, confirming that the gas is primarily hydrogen (Fig. 2a).

The amount of hydrogen produced is plotted as a function of time for CP-ESA and 10AA fibers in Fig. 2b. The results indicate that the amount of hydrogen formed as a function of time can be approximated by a linear relationship. Thus, hydrogen generation rates can be derived using a linear fit and the corresponding effective current for hydrogen generation can be calculated. This data is summarized in Table 1. It is notable that the obtained rates clearly distinguish each carbon paper, indicating that the properties of the given carbon samples affect the reaction rate very significantly. Further experiments were conducted to elucidate the origins of the distinct hydrogen evolution rate.

Table 1
Hydrogen generation rate and corresponding effective current, BET surface area, electrochemical surface area and surface species (at%) obtained by XPS of the carbon paper samples.

	CP-ESA	10AA
H_2 generation rate (μmol min^{-1} g^{-1})	0.17	0.005
Effective current (μA g^{-1})	547	16
BET surface area (BETSA) (m^2 g^{-1})	49.8	1.0
Surface area (micropore) (m^2 g^{-1})	0	0.2
Electrochemical surface area (ECSA) (m^2 g^{-1})	15.4	0.24
ECSA/BETSA (%)	30.9	24.0
H_2 generation rate normalized by ECSA (μmol min^{-1} m^{-2})	0.011	0.021
XPS surface species (at%)		
C	98.4	98.9
O	0.6	0.7
N	1.0	–
F	–	0.4

3.3. Electrochemical surface area and wetting

In general, the rate of reaction is related to the available surface area. However, the BETSA accessed by N_2 gas may not necessarily equal the surface area that is electrochemical active due to capillary forces preventing the liquid to wet the entire porosity. To assess this point, we measured the Electrochemical Surface Area (ECSA) via a capacitance measurement for samples fully immersed in 4 M sulfuric acid. The capacitance of a glassy carbon disk electrode with known area and low surface roughness was measured yielding an area-specific capacitance (23 μF cm^{-2}) typical of the experimental conditions. The ECSA for each sample was calculated based on the measured capacitance and the area-specific capacitance by assuming a similar electrochemical double layer structure for all carbons. An example of the EIS spectrum for the capacitance measurement is shown in Fig. S2. The BETSA represents the surface that N_2 molecules can reach, whereas the capacitance method probes the surface area that is accessible by the solution. The ratio of the ECSA to the BETSA yields a measure of the wetting of the sample. The obtained numbers are listed in Table 1. As indicated in Table 1, 10AA has a lower BETSA by a factor of 50 as compared to CP-

ESA. However, the ECSA of 10AA is lower than that of CP-ESA by a factor of 64 indicating slightly poorer wetting for 10AA. This can be attributed to the presence of micro-pores in 10AA which are detected by nitrogen sorption but which may not be accessible to the electrolyte under ambient pressure. Comparing the hydrogen generation rate normalized by the ECSA (Table 1) suggests the carbon surface of 10AA is more active than that of CP-ESA for hydrogen generation. The surface chemistry was therefore analyzed by XPS for both carbon papers to determine whether surface chemistry of the carbon played a significant role.

3.4. Surface chemistry

The surface chemistry determined by XPS for the starting carbon papers is presented in Fig. 3 and the corresponding atomic concentrations are given in Table 1. Both 10AA and CP-ESA materials have fairly clean surfaces. 10AA has very little O measured (0.7 at%), no N detected and a small amount of F (0.4 at%) in the form of CF_2–CF_2. Similarly, CP-ESA has a very low concentration of O (0.6 at%) but shows a slight amount of N (1.0 at%) characterized in the form of graphitic C_3N species (401 eV). The presence of O in both samples can be related to ether and hydroxyl, and carboxyl or carbonate functionalities. In both cases, there is evidence for π/π^* transition due to the presence of unsaturated carbon bonds, such as in a graphitic carbons, and characterized by a peak 6.7 eV above the main peak at 284.8 eV (291.5 eV) [29] overlapping with the expected response for CF_2–CF_2 in the case of 10AA. The full width at half maximum (FWHM) of the main C1s peak at 284.8 eV is indicative of the degree of the carbon structure ordering, with lower values indicating highly ordered graphitic structures. [30] The FWHM of the main C1s peak for the present carbon papers are equal to 1.34 and 1.35 eV for 10AA and CP-ESA, respectively, which suggests similar carbon ordering. As indicated by XPS analysis, with the exception of small amounts of N (C_3N) for CP-ESA and F (CF_2) for 10AA, the surface chemistry and the carbon nature are fairly similar for the carbon papers studied. No direct evidence was found that surface chemistry is responsible for the higher HER rate of 10AA. It might be that trace metal impurities, which are below the XPS detection limit (0.1 at%) could cause a more active surface. Despite the finding that the impact of surface chemistry is minor in this present work, we would expect that the carbon surface resulting from various fabrication routes may have distinct properties which would affect the HER to some extent. The impact of the surface chemistry on the HER awaits further work to acquire a more detailed data set.

3.5. Implications

To further consider the implications of this HER rate for VRFB system attributes, we, for instance, use the CP-ESA data from Table 1 to estimate the approximate rate at which the cell would become imbalanced. Considering a hypothetical 1 MW h system operating at 1 MW, and using the voltage per cell of 1.4 V entails a total current of $\sim 7 \times 10^5$ A. If we operate at 100 mA cm^{-2}, we need 7×10^6 cm^2 of the most active carbon (c.a. 8 mg cm^{-2}), which generates $\sim 6 \times 10^5$ μmol of hydrogen per hour, or 1.2×10^5 C h^{-1}. The current from vanadium charging corresponds to roughly 2.5×10^9 C h^{-1}, so the system is out

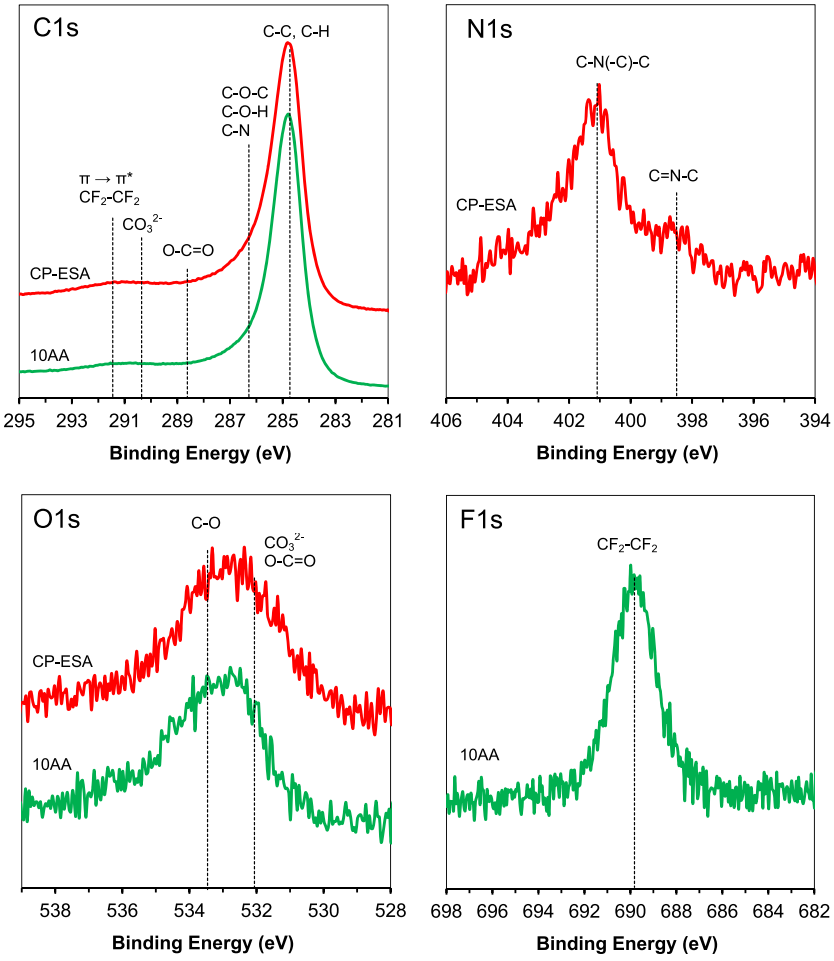

Fig. 3. High resolution C1s, N1s, O1s and F1s X-ray photoelectron spectra of the starting carbon samples. Assignments are indicated in the figures.

of balance at the rate of 0.005% h^{-1} approximately. Note that this is a substantial overestimation because the time spent fully charged—the SOC of maximum hydrogen evolution—is a small fraction of the total duty cycle and the current from the HER will drop exponentially with voltage. Nonetheless, such a rate would require weekly rebalancing to the tune of ~1%. We also point out that the higher total surface area results in substantial increases in performance. Higher operating current density translates directly to lower needed total surface area and a proportionally lower rate.

4. Conclusions

The hydrogen evolution taking place in the negative electrode environment of the VRFB has been studied. Two types of carbon paper examined by buoyancy test have been found to yield distinct hydrogen formation rates. The nitrogen adsorption method, capacitance and XPS measurements have been carried out to further characterize the BETSA, the ECSA and the surface chemistry of each carbon material.

With comparable surface chemistry for 10AA and CP-ESA, we attribute the 50-fold difference in hydrogen formation rate to the distinct available electrochemical surface area. As the performance of the VRFB is significantly improved by adopting high surface area and high porosity electrode materials, the rate of the side reactions in the RFB may scale up proportionally and be partly responsible for the capacity fade. Here, we address this issue by correlating the structure–property relationships of various carbon materials toward hydrogen gas evolution.

Acknowledgments

The authors gratefully acknowledge the support of the US Department of Energy Office of Electricity Storage Systems Program directed by Dr. Imre Gyuk and the University of Tennessee Governor's Chair Fund for support of this work. Dr. Hui Zhou is gratefully acknowledged for his support during SEM collection. This work was partially supported by the U.S. Department of Energy's (DOE) Office of Basic Energy Sciences (BES), Materials Sciences and Engineering Division (LB, GMV).

Appendix A. Supplementary data

Supplementary data related to this article can be found at http://dx.doi.org/10.1016/j.jpowsour.2013.09.125.

References

[1] J. Liu, J.-G. Zhang, Z. Yang, J.P. Lemmon, C. Imhoff, G.L. Graff, L. Li, J. Hu, C. Wang, J. Xiao, G. Xia, V.V. Viswanathan, S. Baskaran, V. Sprenkle, X. Li, Y. Shao, B. Schwenzer, Adv. Energy Mater. 23 (2013) 929–946.
[2] Z. Yang, J. Zhang, M.C.W. Kintner-Meyer, X. Lu, D. Choi, J.P. Lemmon, J. Liu, Chem. Rev. 111 (2011) 3577–3613.
[3] A.Z. Weber, M.M. Mench, J.P. Meyers, P.N. Ross, J.T. Gostick, Q. Liu, J. Appl. Electrochem. 41 (2011) 1137–1164.
[4] Q. Huang, H. Li, M. Grätzel, Q. Wang, Phys. Chem. Chem. Phys. 15 (2013) 1793–1797.
[5] C. Ponce de León, A. Frías-Ferrer, J. González-García, D.A. Szánto, F.C. Walsh, J. Power Sources 160 (2006) 716–732.
[6] M. Skyllas-Kazacos, J. Electrochem. Soc. 133 (1986) 1057.
[7] M. Kazacos, M. Cheng, M. Skyllas-Kazacos, J. Appl. Electrochem. 20 (1990) 463–467.
[8] E. Sum, M. Skyllas-Kazacos, J. Power Sources 15 (1985) 179–190.
[9] M. Rychcik, M. Skyllas-Kazacos, J. Power Sources 19 (1987) 45–54.
[10] C. Fabjan, J. Garche, B. Harrer, L. Jörissen, C. Kolbeck, F. Philippi, G. Tomazic, F. Wagner, Electrochim. Acta 47 (2001) 825–831.
[11] A. Di Blasi, O. Di Blasi, N. Briguglio, A.S. Aricò, D. Sebastián, M.J. Lázaro, G. Monforte, V. Antonucci, J. Power Sources 227 (2013) 15–23.
[12] S. Kim, J. Yan, B. Schwenzer, J. Zhang, L. Li, J. Liu, Z.G. Yang, M.A. Hickner, Electrochem. Commun. 12 (2010) 1650–1653.
[13] D.S. Aaron, Q. Liu, Z. Tang, G.M. Grim, A.B. Papandrew, A. Turhan, T.A. Zawodzinski, M.M. Mench, J. Power Sources 206 (2012) 450–453.
[14] W. Zhang, J. Xi, Z. Li, H. Zhou, L. Liu, Z. Wu, X. Qiu, Electrochim. Acta 89 (2013) 429–435.
[15] B. Li, M. Gu, Z. Nie, Y. Shao, Q. Luo, X. Wei, X. Li, J. Xiao, C. Wang, V. Sprenkle, W. Wang, Nano Lett. 13 (2013) 1330–1335.
[16] C. Fujimoto, S. Kim, R. Stains, X. Wei, L. Li, Z.G. Yang, Electrochem. Commun. 20 (2012) 48–51.
[17] B. Schwenzer, J. Zhang, S. Kim, L. Li, J. Liu, Z. Yang, ChemSusChem 4 (2011) 1388–1406.
[18] D. Chen, S. Kim, V. Sprenkle, M.A. Hickner, J. Power Sources 231 (2013) 301–306.
[19] Z. Mai, H. Zhang, H. Zhang, W. Xu, W. Wei, H. Na, X. Li, ChemSusChem 6 (2013) 328–335.
[20] L. Li, S. Kim, W. Wang, M. Vijayakumar, Z. Nie, B. Chen, J. Zhang, G. Xia, J. Hu, G. Graff, J. Liu, Z. Yang, Adv. Energy Mater. 1 (2011) 394–400.
[21] J. Xi, Z. Wu, X. Qiu, L. Chen, J. Power Sources 166 (2007) 531–536.
[22] Q. Luo, L. Li, W. Wang, Z. Nie, X. Wei, B. Li, B. Chen, Z. Yang, V. Sprenkle, ChemSusChem 6 (2013) 268–274.
[23] A.H. Whitehead, M. Harrer, J. Power Sources 230 (2013) 271–276.
[24] A.A. Shah, H. Al-Fetlawi, F.C. Walsh, Electrochim. Acta 55 (2010) 1125–1139.
[25] C.H. Fujimoto, M.A. Hickner, C.J. Cornelius, D.A. Loy, Macromolecules 38 (2005) 5010–5016.
[26] D. Xing, S. Zhang, C. Yin, B. Zhang, X. Jian, J. Memb. Sci. 354 (2010) 68–73.
[27] D. Aaron, C.-N. Sun, M. Bright, A.B. Papandrew, M.M. Mench, T.A. Zawodzinski, ECS Electrochem. Lett. 2 (2013) A29–A31.
[28] C.-N. Sun, F.M. Delnick, D.S. Aaron, A.B. Papandrew, M.M. Mench, T.A. Zawodzinski, ECS Electrochem. Lett. 2 (2013) A43–A45.
[29] D. Briggs, Practical Surface Analysis, second ed., John Wiley & Sons, Chichester, 1990.
[30] T. Takahagi, A. Ishitani, Carbon 26 (1988) 389–395.